

5-1-2005

DFT/RDFT Filter Banks with Symmetric Zero-Phase Nonoverlapping Analysis/Synthesis Filters and Applications

Okan K. Ersoy

Follow this and additional works at: <http://docs.lib.purdue.edu/ecetr>

Ersoy, Okan K., "DFT/RDFT Filter Banks with Symmetric Zero-Phase Nonoverlapping Analysis/Synthesis Filters and Applications" (2005). *ECE Technical Reports*. Paper 9.
<http://docs.lib.purdue.edu/ecetr/9>

This document has been made available through Purdue e-Pubs, a service of the Purdue University Libraries. Please contact epubs@purdue.edu for additional information.

DFT / RDFT FILTER BANKS WITH
SYMMETRIC ZERO-PHASE
NONOVERLAPPING
ANALYSIS / SYNTHESIS FILTERS AND
APPLICATIONS

OKAN K. ERSOY

TR-ECE 05-07
MAY 2005

PURDUE
UNIVERSITY

SCHOOL OF ELECTRICAL
AND COMPUTER ENGINEERING
PURDUE UNIVERSITY
WEST LAFAYETTE, IN 47907-2035

**DFT/RDFT Filter Banks with
Symmetric Zero-Phase Nonoverlapping
Analysis/Synthesis Filters and Applications**

Okan K. Ersoy

TR-ECE 05-07
May 2005

School of Electrical and Computer Engineering
465 Northwestern Ave
Purdue University
West Lafayette, IN 47907-2035

TABLE OF CONTENTS

ABSTRACT	3
1. INTRODUCTION.....	5
2. DFT FILTER BANKS.....	7
2.1 Zero-Phase Filter.....	7
2.2 DFT Filter Bank.....	7
3. SYMMETRIC ZERO-PHASE FIR ANALYSIS/SYNTHESIS FILTERS.....	11
4. SUBBAND REPRESENTATION WITH THE DFT FILTER BANKS WITH NON-OVERLAPPING ZERO-PHASE ANALYSIS/SYNTHESIS FILTERS.....	13
4.1 DFT and RDFT.....	13
4.2. Analysis by Ideal LP Filtering and Decimation.....	14
4.3. Lowpass Reconstruction in the Synthesis Bank.....	16
4.4 Highpass Reconstruction in the Synthesis Bank.....	17
4.5 Digital Filter Banks with Generalized Non-Ideal Analysis/Synthesis Filters.....	17
5. TREE SUBBAND REPRESENTATION.....	19
6. APPLICATIONS.....	21
6.1 1-D Subband Decomposition.....	21
6.2 Image Fusion.....	22
6.3.1 Image Set 1.....	23
6.3.2. Image Set 2.....	27
6.4 Fusion of Remote Sensing Images.....	33
7. CONCLUSIONS.....	39
ACKNOWLEDGEMENT.....	40
REFERENCES	41

ABSTRACT

Digital filter banks satisfying perfect reconstruction (PR) condition are very useful in many applications. In this report, new filter bank structures related to the complex and real discrete Fourier transforms (DFT and RDFT) are introduced, and their performance in applications such as image fusion are investigated as compared to wavelets.

The importance of zero-phase filter banks has been increasing since they can be effectively used within filter banks without time shift (or space shift in 2-D). The art of designing zero-phase low pass and high pass analysis filters is well established. There is also no phase distortion occurring within the filter banks. For a real input signal, analysis/synthesis banks with such filtering always give a real output signal. Consequently, the proposed DFT/RDFT filter banks with symmetric zero-phase analysis filters may be suitable for a wide range of applications in signal and image processing.

The method developed was used in 1-D, and 2-D subband decomposition tasks. Image fusion was especially the application studied in detail. In terms of performance, the results with the new method was better than the results obtained with the wavelet approach using Daubechies 1 (Haar) wavelet in all the applications comparatively studied .

1. INTRODUCTION

Digital filter banks have been widely applied in many areas such as speech and image processing, especially in the form of subband representation. In these applications, the structure of maximally decimated filter bank has been popularly used. Among many types of digital filter banks, cosine-modulated filter banks with PR have become popular due to simple implementation and low cost [1]-[4]. Another popular digital filter bank called DFT polyphase filter bank [3] has one critical problem. It suffers from not being able to cancel aliasing caused by subsampling the subband signals although it provides efficient computation. This disadvantage has been overcome by a modification of filter bank structure, called MDFT filter bank [5]-[7]. The MDFT filter bank with linear-phase analysis filters uses either real or imaginary part separately in the subbands,

Zero-phase filters are useful in the realization of digital filter banks and wavelets [8]-[11]. The zero-phase filter bank design method by a change of variable was introduced by Herrmann [12]. DFT filter banks with zero-phase analysis filters have no phase distortion due to zero-phase property of analysis filters. However, if we use symmetric zero-phase analysis filters, filter banks can not satisfy perfect reconstruction condition. This disadvantage is overcome by the proposed method..

In this report, we propose a method to cancel aliasing within the filter banks with the nonoverlapping symmetric zero-phase analysis filters and thereby achieve perfect reconstruction. Vetterli's theorem shows the conditions for perfect reconstruction in the frequency domain for the DFT filter bank with two-channel maximally decimated filter bank structure [11]. However, the theorem is not valid for the maximally decimated filter bank with symmetric zero-phase analysis filters since aliasing can not be cancelled within the filter bank due to the symmetric property of analysis filters, causing problems at $\omega=\pi/2$. This disadvantage is removed with the proposed method.

The report is organized in seven sections. Section 2 describes briefly zero-phase filters and DFT filter banks with PR conditions. Section 3 is on symmetric, zero-phase analysis/synthesis filters with perfect reconstruction property. Section 4 discusses the proposed DFT/RDFT method with non-overlapping symmetric zero-phase analysis/synthesis filters. Section 5 is a brief discussion of tree subband representation. Section 6 starts with the 1-D decomposition of a speech signal to verify the PR property of the method. Then, image fusion applications are investigated, in comparison to the wavelet method. Section 7 covers conclusions.

2. DFT FILTER BANKS

This section discusses briefly the concept of zero-phase filter, which is a special case of linear-phase filter. We are interested in the symmetric zero-phase filter which means the frequency response of the zero-phase filter is symmetric along π . Then, the transfer function of the symmetric zero-phase filter is real in the frequency domain. The DFT filter bank is also introduced with the frequency domain analysis for explaining aliasing cancellation and PR.

2.1 Zero-Phase Filter

Zero-phase filter is a special case of linear-phase filter where the phase slope is zero. The real impulse response $h(n)$ of a zero-phase filter satisfies

$$h[n] = h[N - n] \quad (2.1)$$

where N is the length of impulse response $h(n)$. In the frequency domain, the frequency response (transfer function) is real and symmetric along π .

2.2 DFT Filter Bank

Fig.2.1 shows the two-channel maximally decimated DFT filter bank. The $H_k(z)$ and $F_k(z)$ are analysis and synthesis filters, respectively. The symbol “ $\downarrow 2$ ” represents decimation by a factor of 2, whereas “ $\uparrow 2$ ” describes the corresponding interpolation by a factor of 2. When the factors of decimation and interpolation are the same in the filter bank, we call it maximally decimated filter bank.

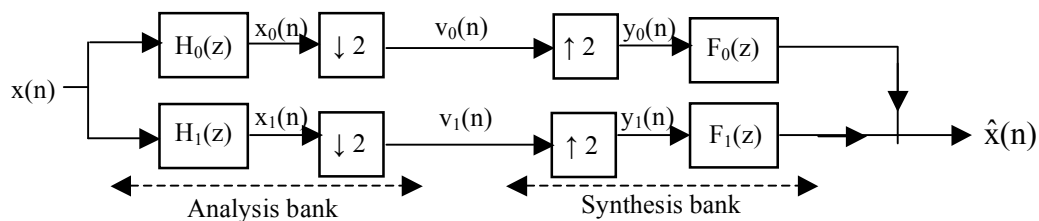


Figure 1. Two-channel maximally decimated filter bank.

The PR conditions can be expressed in the frequency domain. In terms of the z -transform, we have

$$X_0(z) = H_0(z)X(z), \quad X_1(z) = H_1(z)X(z) \quad (2.2)$$

The decimated signals $v_0(n)$ and $v_1(n)$ in the z -domain are

$$V_0(z) = \frac{1}{2} [X_0(z^{1/2}) + X_0(-z^{1/2})], \quad V_1(z) = \frac{1}{2} [X_1(z^{1/2}) + X_1(-z^{1/2})] \quad (2.3)$$

The second terms of $V_0(z)$ and $V_1(z)$ in Eq.(2.3) represent aliasing caused by the decimation of the signals. By interpolation in the synthesis bank, we get

$$\begin{aligned} Y_0(z) &= V_0(z^2) = \frac{1}{2} [X_0(z) + X_0(-z)] = \frac{1}{2} [H_0(z)X(z) + H_0(-z)X(-z)] \\ Y_1(z) &= V_1(z^2) = \frac{1}{2} [X_1(z) + X_1(-z)] = \frac{1}{2} [H_1(z)X(z) + H_1(-z)X(-z)] \end{aligned} \quad (2.4)$$

The reconstructed signal is expressed as

$$\hat{X}(z) = F_0(z)Y_0(z) + F_1(z)Y_1(z) \quad (2.5)$$

Substituting from Eq.(2.4) and rearranging, we finally get

$$\begin{aligned} \hat{X}(z) &= \frac{1}{2} [H_0(z)F_0(z) + H_1(z)F_1(z)]X(z) + \frac{1}{2} [H_0(-z)F_0(z) + H_1(-z)F_1(z)]X(-z) \\ &= T(z)X(z) + A(z)X(-z) \end{aligned} \quad (2.6)$$

where $T(z)$ is the distortion function and $A(z)$ is the aliasing function. Using matrix notation, the last result can be written as

$$\hat{X}(z) = \frac{1}{2} [X(z) \quad X(-z)] \begin{pmatrix} H_0(z) & H_1(z) \\ H_0(-z) & H_1(-z) \end{pmatrix} [F_0(z) \quad F_1(z)]^T \quad (2.7)$$

When $\hat{X}(z)$ is equal to $X(z)$, we get the original signal back from the filter bank. So the first term in Eq.(2.6) should be $X(z)$ and second term in Eq.(2.6) should be cancelled for PR. In matrix representation, this conclusion can be written as [12]

$$\begin{pmatrix} H_0(z) & H_1(z) \\ H_0(-z) & H_1(-z) \end{pmatrix} [F_0(z) \quad F_1(z)]^T = [2 \quad 0]^T \quad (2.8)$$

The following choice of $F_0(z)$ and $F_1(z)$ cancels aliasing:

$$F_0(z) = H_1(-z), F_1(z) = -H_0(-z) \quad (2.9)$$

Then, the distortion and aliasing functions are given by

$$A(z) = \frac{1}{2} [H_0(-z)F_0(z) + H_1(-z)F_1(z)] = \frac{1}{2} [H_0(-z)H_1(-z) - H_1(-z)H_0(-z)] = 0 \quad (2.10)$$

$$T(z) = \frac{1}{2} [H_0(z)F_0(z) + H_1(z)F_1(z)] = \frac{1}{2} [H_0(z)H_1(-z) - H_1(z)H_0(-z)] \quad (2.11)$$

3. SYMMETRIC ZERO-PHASE FIR ANALYSIS/SYNTHESIS FILTERS

Optimum FIR equiripple linear-phase filter design scheme was introduced by Parks and McClellan [13]. When the impulse response $h(n)$ satisfies Eq.(1), the frequency response of FIR linear-phase filter becomes the real-valued frequency response given by

$$H(\omega) = \sum_{k=0}^{N-1} \alpha[k] \cos(\omega k) \quad (3.1)$$

where $\{\alpha(k)\}$ represents the parameters of the filter. Examples of linear phase filter transfer functions are shown in Figure 2. In the analysis bank, two zero-phase filters $H_0(z)$ and $H_1(z)$ are used, where $H_0(z)$ is a low pass filter, and $H_1(z)$ is a high pass filter. For example, the discrete-time filter transfer functions in the DFT/RDFT representation used in this paper can be chosen as

$$H_0[k] = 0.58 + 0.5 \cos\left(\frac{2\pi k}{N}\right) - 0.08 \cos\left(\frac{4\pi k}{N}\right) \quad k = 0, 1, \dots, N-1 \quad (3.2)$$

$$H_1[k] = 0.42 - 0.5 \cos\left(\frac{2\pi k}{N}\right) + 0.08 \cos\left(\frac{4\pi k}{N}\right) \quad k = 0, 1, \dots, N-1 \quad (3.3)$$

The corresponding LP and HP filter transfer functions are shown in Figure 2(a), respectively. If we choose $H_0(k) = 0.5 + 0.5 \cos(2\pi k/N)$, $H_1(k) = 0.5 - 0.5 \cos(2\pi k/N)$, then $H_0(k)$ and $H_1(k)$ are symmetric around $\pi/2$ as shown in Figure 2(b). The coefficients of $H_0(k)$ and $H_1(k)$ are all real and positive valued. In the zero-phase filter design used in this report, we keep the relationship between $H_0(k)$ and $H_1(k)$ as

$$H_0[k] + H_1[k] = 1 \quad k = 0, 1, \dots, N-1 \quad (3.4)$$

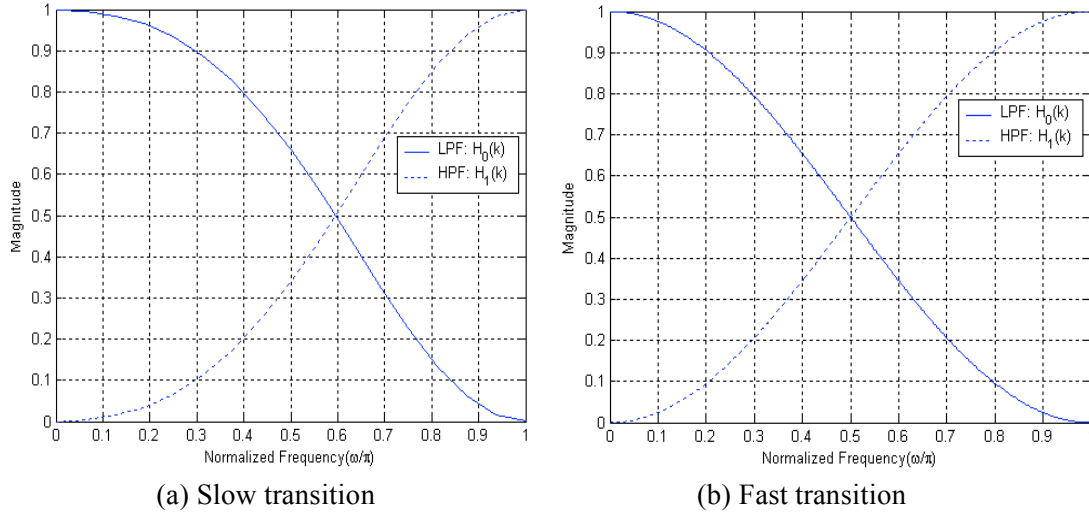


Figure 2. Examples of LPF and HPF in the analysis and synthesis bank.

For linear-phase filters, when $H_0(k)$ is a low pass filter, $1-H_0(k)$ does not necessarily mean a high pass filter. But, this relationship holds for zero-phase filters using Eq.(3.4). When $H_0(k)$ is an ideal LP filter, then $H_1(k)$ becomes an ideal HP filter. When $H_0(k)$ is an ideal BP filter, then $H_1(k)$ is an ideal BR filter. Figures 3(a) and 3(b) show this relationship.

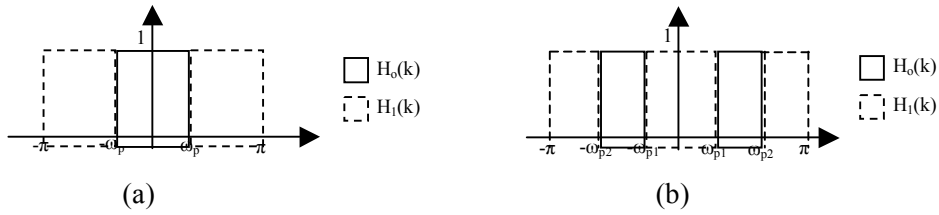


Figure.3. (a) Ideal LP and HP zero-phase filters, (b) Ideal BP and BR zero-phase filters.

Four properties of symmetric zero-phase analysis bank filters are given by

$$(1) H_0(k) = H_0(N-k), H_1(k) = H_1(N-k), \quad k=0,1,2,\dots,N-1$$

This is the symmetric property of zero-phase filters in the frequency domain.

$$(2) H_0(k) + H_1(k) = 1 \leftrightarrow h_0(n) + h_1(n) = \delta(n), \quad k=0,1,2,\dots,N-1$$

From given $H_0(k)$, $H_1(k)$ can be chosen as $1 - H_0(k)$. If $H_0(k)$ is symmetric in the frequency domain, then $H_1(k)$ is also symmetric in the frequency domain. Letting $h(n) = h_0(n) + h_1(n) \leftrightarrow H(k) = H_0(k) + H_1(k)$,

We have

$$h(n) = \sum_{k=0}^{N-1} H(k)e^{j2\pi kn/N} = \sum_{k=0}^{N-1} 1 \cdot e^{j2\pi kn/N} = \delta(n)$$

Therefore, $H_0(k) + H_1(k) = 1 \leftrightarrow h_0(n) + h_1(n) = \delta(n)$

$$(3) X_0(k) + X_1(k) = X(k) \leftrightarrow x_0(n) + x_1(n) = x(n), \quad k=0,1,2,\dots,N-1$$

In the frequency domain, $X_0(k) = H_0(k)X(k)$, $X_1(k) = H_1(k)X(k)$, and $X_0(k) + X_1(k) = H_0(k)X(k) + H_1(k)X(k) = [H_0(k) + H_1(k)] X(k) = X(k)$ by property (2).

Computing IDFT on both sides, $x_0(n) + x_1(n) = x(n)$

$$(4) v_0(n) + v_1(n) = x(2n)$$

Since $x_0(n) + x_1(n) = x(n)$, it is true that $v_0(n) + v_1(n) = x(2n)$.

4. SUBBAND REPRESENTATION WITH THE DFT/RDFT FILTER BANKS AND NON-OVERLAPPING ZERO-PHASE ANALYSIS/SYNTHESIS FILTERS

In this section, we show a method to eliminate aliasing without changing the filter bank structures with the ideal LP and HP analysis filters and expand it to the non-ideal LP and HP analysis filters. We use non-overlapping zero-phase analysis filters.

Fig.4(a) is an example of non-overlapping frequency response for the analysis filter as compared to Fig.4(b) which is an example of overlapping analysis filter discussed in the previous section.

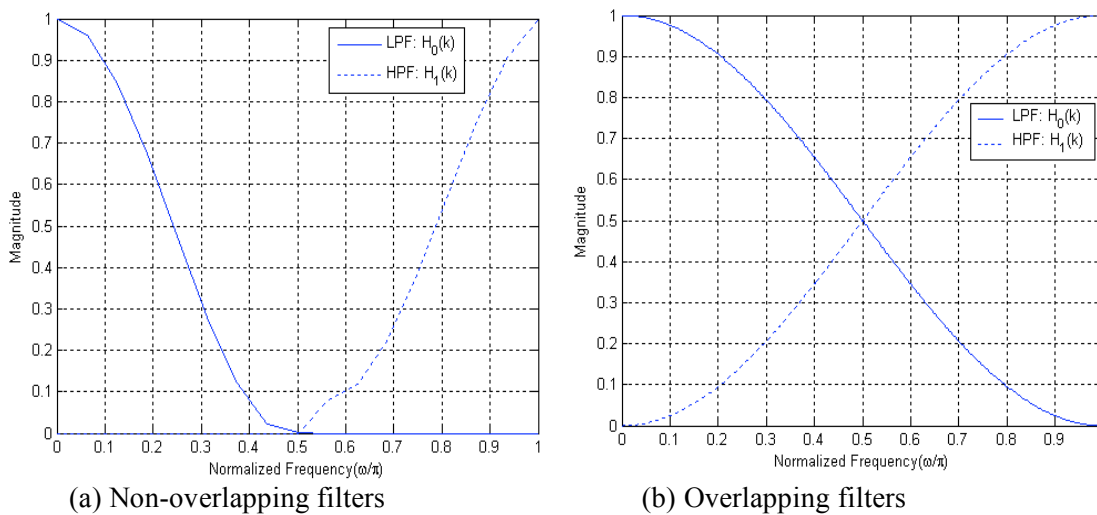


Figure 4. LP and HP filters in the analysis bank.

4.1 DFT and RDFT

The 1-D discrete Fourier transform DFT of a signal $x(n)$ can be written as [14]

$$X[k] = \sum_{n=0}^{N-1} x[n] e^{-j2\pi nk/N} \quad k = 0, 1, \dots, N-1 \quad (4.1)$$

where N is the signal length. The signal is synthesized by the inverse DFT (IDFT) as

$$x[n] = \frac{1}{N} \sum_{k=0}^{N-1} X[k] e^{j2\pi nk/N} \quad n = 0, 1, \dots, N-1 \quad (4.2)$$

The DFT yields complex results. When the input data is real, the output actually has complex conjugate symmetry, hence half of the output data is redundant. If care is not taken, this means twice as many computations are generated.

The real DFT (RDFT) totally avoids redundancy, and has real output for real input [15], [16]. It is given by

$$X[k] = 2w[k] \sum_{n=0}^{N-1} x[n] \cos(2\pi nk/N + \theta[k]) \quad k = 0, 1, \dots, N-1 \quad (4.3)$$

The inverse RDFT (IRDFT) is given by

$$x[n] = \frac{1}{N} \sum_{k=0}^{N-1} X[k] \cos(2\pi nk/N + \theta[k]) \quad n = 0, 1, \dots, N-1 \quad (4.4)$$

where

$$\theta[k] = \begin{cases} 0 & 0 \leq k \leq N/2 \\ \pi & N/2 < k \leq N \end{cases} \quad (4.5)$$

$$w[k] = \begin{cases} 1/2 & k = 0 \text{ or } N/2 \\ 1 & \text{otherwise} \end{cases} \quad (4.6)$$

Both the DFT and the RDFT can be equivalently used to compute circular convolution and in filtering as further discussed below. When the filter is symmetric zero-phase filter, this equivalence is even more striking since the fast fft routine to compute the DFT in a program package can be replaced by the fast rfft

routine to compute the RDFT in the same program package to convert from the DFT to the RDFT processing or vice versa, without any further changes. Because of this equivalence, the theory in subsequent sections is discussed in terms of the DFT only.

4.2. Analysis by Ideal LP Filtering and Decimation

The $X_{LP}(k)$ is defined as the LP filtered DFT of $x(n)$ and can be expressed as

$$X_{LP}[k] = \begin{cases} X[k] & 0 \leq k \leq K, N - K \leq k < N \\ 0 & \text{otherwise} \end{cases} \quad (4.7)$$

The lowpass signal is given by

$$x_{LP}[n] = \frac{1}{N} \sum_{k=0}^{N-1} X_{LP}[k] e^{j2\pi nk / N} \quad (4.8)$$

We will choose $K=N/4$ below. The decimated signal $x'_{LP}(n)$ can be expressed as

$$\begin{aligned} x'_{LP}[n] &= x_{LP}[2n] = \frac{1}{N} \sum_{k=0}^{N-1} X_{LP}[k] e^{j2\pi nk / N} \\ &= \frac{1}{N} \sum_{k=0}^{N/2-1} X_{LP}[k] e^{j2\pi nk / N} + \sum_{k=0}^{N/2-1} X_{LP}[k + N/2] e^{j2\pi nk / N} \end{aligned} \quad (4.9)$$

We next consider the highpass signal $x_{HP}(n)$. Its DFT is given by

$$X_{HP}[k] = \begin{cases} X[k] & K < k < N - K \\ 0 & \text{elsewhere} \end{cases} \quad (4.10)$$

where $K \leq N/4$.

$x_{HP}(n)$ has IDFT synthesis given by

$$x_{HP}[n] = \sum_{k=0}^{N-1} X_{HP}[k] e^{j2\pi nk / N} \quad (4.11)$$

For a real signal $x(n)$,

$$X_{HP}[k] = X_{HP}^*[N - k] \quad (4.12)$$

Decimated signal $x'_{HP}(n)$ can be expressed as

$$x'_{HP}[n] = x_{HP}[2n] = \sum_{k=0}^{N-1} X_{HP}[k] e^{j2\pi nk / (N/2)} \quad (4.13)$$

Letting $k' = k - K$, $k = k' + K$, we get

$$x'_{HP}[n] = \sum_{k'=0}^{N-2K} X_{HP}[k' + K] e^{j2\pi n(k' + K) / (N/2)} \quad (4.14)$$

We assume $K = N/4$ below. Then,

$$x'_{HP}[n] = \sum_{k'=0}^{N/2} X_{HP}[k' + K] e^{j2\pi nk' / (N/2)} \quad (4.15)$$

Using $X_{HP}[k' + K] = X_{HP}^*[N - k' - K]$, we can express Eq.(4.15) in a similar form to Eq.(4.8).

Eq.(4.15) explains the process of ideal HP filtering and decimation in the analysis bank.

4.3. Lowpass Reconstruction in the Synthesis Bank

For a real signal $x(n)$, it is true that

$$X_{LP}[k] = X_{LP}^*[N - k] \quad (4.16)$$

Using Eqs. (4.9) and (4.10), $x'_{LP}[n]$ can be written as

$$x'_{LP}[n] = \frac{2}{N} \sum_{k=1}^{N/2-1} X_{LP1}[k] [\cos(2\pi nk / (N/2)) + \sin(2\pi nk / (N/2))] + \frac{1}{N} [X_{LP}[0] + X_{LP}[N/2]] \quad (4.17)$$

where

$$X_{LP}[k] = X_{LP1}[k] - jX_{LP0}[k] \quad (4.18)$$

For the reconstruction in the synthesis bank, we need to compensate the magnitude reduction by a factor of 2 due to the decimation in the analysis bank. Then, we have

$$2X'_{LP}[k] = \begin{cases} X_{LP}[k] & 0 \leq k < N/4 \\ 2\text{Re}\{X_{LP}[k]\} & k = N/4 \\ X_{LP}^*[N/2 - k] & N/4 < k < N/2 \end{cases} \quad (4.19)$$

To reconstruct $X_{LP}[k]$ from $2X'_{LP}[k]$, we need scaling by a factor of 2 and imaginary part of $X_{LP}[k]$ at $k=N/4$ as seen in Eq.(4.9).

Then, the reconstruction of the lowpass signal is achieved as follows:

1. High frequency components ($N/4 < k < 3N/4$) are filled with zeros.
2. Low frequency components ($0 \leq k < N/4$) are filled with the components of $2 \cdot X'_{LP}(k)$ in $0 \leq k < N/4$.
3. The component at $k=N/4$ is recovered by using the imaginary part of $2X_{LP}(N/4)$.
4. Low frequency components ($3N/4 \leq k < N$) can be found as the complex conjugate of the low frequency components ($0 < k \leq N/4$) in the case of the DFT.
5. $x_{LP}(n)$ is recovered by computing the IDFT of X .

4.4 Highpass Reconstruction in the Synthesis Bank

For the interpolation in the synthesis bank, we need to consider the exponential term in Eq.(4.17). That term oscillates between 1 and -1 for integer n . Also, we need to compensate the magnitude reduction by a factor of 2 due to the decimation in the analysis bank. We have

$$2X'_{HP}[k] = \begin{cases} 0 & k = 0 \\ X_{HP}[k + K] & N/4 < k < N/2 \end{cases} \quad (4.21)$$

Then, the interpolation operation is processed in the frequency domain as follows:

- (1) High frequency components ($N/4 < k < 3N/4$) are filled with the components of $2 \cdot X'_{HP}(k)$ in $N/4 < k < N/2$.
- (2) Other low frequency components are set to zero.

After this interpolation is done in the frequency domain, we can recover $x_{HP}(n)$ by computing its IDFT.

4.5 Digital Filter Banks with Generalized Non-Ideal Analysis/Synthesis Filters

We discussed the ideal LP and HP filtering, decimation and interpolation with the filter bank in the previous section. Now, we can expand this method to the non-ideal case of non-overlapping LP and HP analysis filters shown in Figure 4(a). We can apply these filters by point-wise multiplication in the frequency domain. When we do interpolation in the synthesis bank, we need to compensate magnitude due to the use of non-ideal LP and HP analysis filters.

We define the following:

x: signal vector

T: transform matrix

H_{LP} : Non-ideal LP filter matrix

H_{HP} : Non-ideal HP filter matrix

We assume that all the matrices are invertible. In the analysis bank prior to the decimation, the signals can be expressed as

$$y_{LP} = T^{-1}H_{LP}Tx \quad (4.22)$$

$$y_{HP} = T^{-1}H_{HP}Tx \quad (4.23)$$

Next, we decimate the signal in the analysis bank. H_{LP} is a LP analysis filter and zero when $K < k \leq N/2$, and H_{HP} is a HP analysis filter and zero when $k \leq K$ where $K = N/4$ is used in this report. This property guarantees non-overlapping analysis filters. In the synthesis bank, after the interpolation, we need to compensate for magnitude, using the inverse of H_{LP} and H_{HP} .

For the lowpass signal, this can be expressed as

$$X'_{LP} = \begin{cases} H_{LP}^{-1}Ty_{LP} & 0 \leq k \leq N/4 \\ 0 & k > N/4 \end{cases} \quad (4.24)$$

where X'_{LP} is the LP filtered signal in the frequency domain and H_{LP}^{-1} is the inverse matrix of H_{LP} . Then, we reconstruct the lowpass signal by computing the inverse transform of X'_{LP} .

For the HP analysis filters, we have

$$X'_{HP} = \begin{cases} H_{HP}^{-1} T y_{HP} & N/4 \leq k \leq N/2 \\ 0 & k \leq N/4 \end{cases} \quad (4.25)$$

where X'_{HP} is the HP filtered signal in the frequency domain, and H_{HP}^{-1} is the inverse matrix of H_{HP} . Then, we reconstruct the highpass signal as discussed in Section 4.3. The original signal is recovered by adding the reconstructed lowpass and highpass signals.

The methodology discussed above is valid with any invertible transform T as long as interpolation can be done on the decimated signals without loss.

5. TREE SUBBAND REPRESENTATION

The process of decomposing the signal into lowpass and highpass components can be done recursively a number of times. The common procedure is to repeat the process on the lowpass component a number of times, or possibly until reaching the size of 1 (if the initial size is a power of 2). This procedure is the same whether filter banks or wavelets are used.

For 2-D signals like images, LP/HP filtering and decimation are applied in two directions, row-wise direction and column-wise direction or vice versa. There are four possible cases, LL, LH, HL, HH where L means low pass filtering and H means high pass filtering. For example, the first L or H is applied in the row-wise direction, then the second L or H is applied in the column-wise direction. The size of image in each quadrant is 25% of the size of the original image since decimation is applied in both row and column directions. For multilevel decomposition, the process is recursively applied to the 1st quadrant image at each decomposition level. Then, the maximum, or the minimum, or the average gray scale pixel values are chosen in the subband domain.

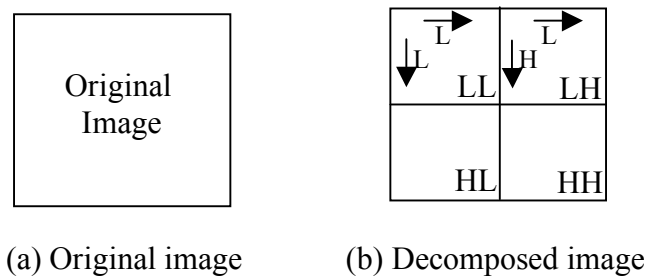


Figure 5. Image decomposition.

6. APPLICATIONS

In this section, we initially apply the DFT/RDFT based zero-phase filter bank developed in the previous sections to a chosen speech signal and verify PR. Next the method is used in the applications of image fusion. The performance of the method is investigated in comparison to the performance of the wavelet method in which the wavelet used was the Daubechies wavelet 1 (the Haar wavelet).

6.1 1-D Subband Decomposition

As an example, Figure 6 shows the speech signal of utterance ‘start’. The length of the sequence is 8848. The proposed algorithm was used with non-overlapping real symmetric zero-phase analysis filters for testing PR. The filters shown in Figure 4(a) was used as LP and HP analysis filters. The output of analysis bank is shown in Figure 7 and Figure 8, respectively. As seen in these figures, low frequency components are dominant in the speech signal. Figure 9 is the reconstructed speech signal, and the mean square error (MSE) of reconstruction is $5.2118e-10$.

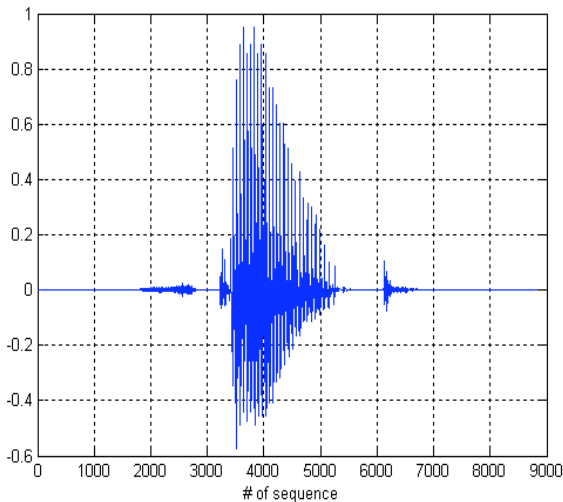


Figure 6. Signal utterance ‘start’.

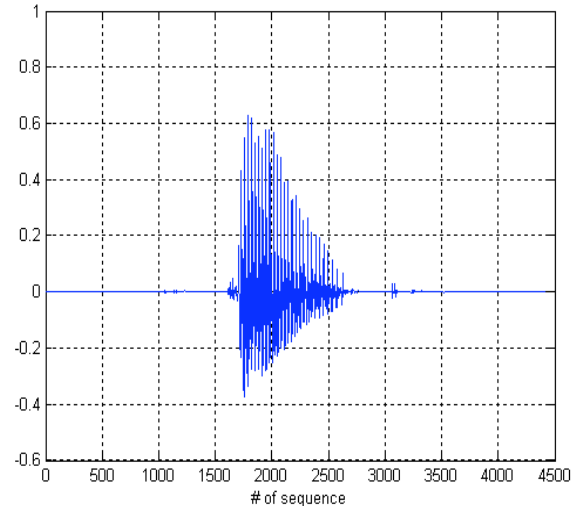


Figure 7. LP filtered/decimated signal.

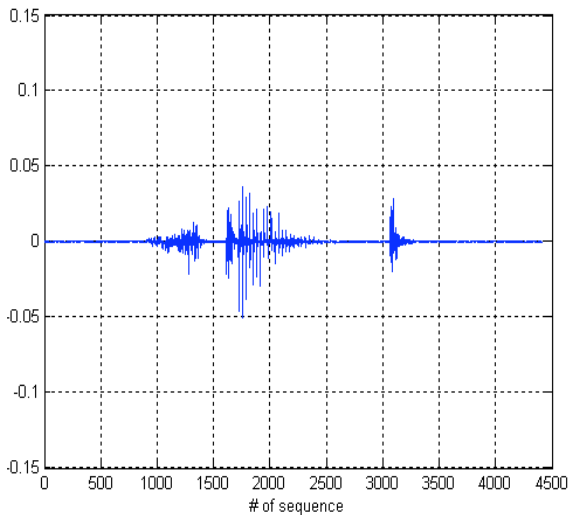


Figure 8. HP filtered/decimated signal.

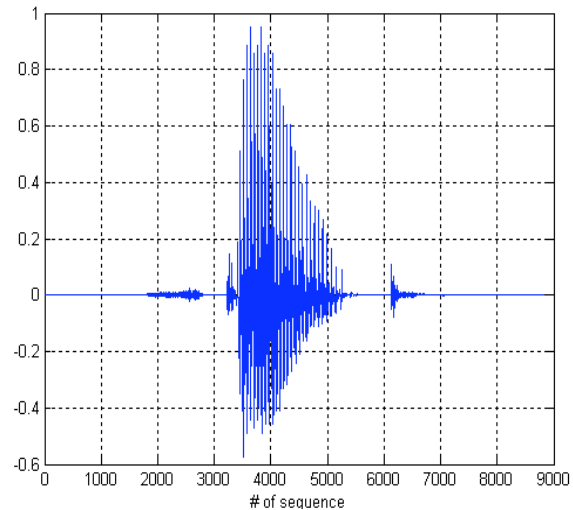


Figure 9. Reconstructed signal.

6.2 Image Fusion

Image fusion is the process of combining complementary information from multiple image sources to obtain a new image which is more suitable for human and machine perception or further image processing applications such as segmentation, feature extraction and object recognition [17]-[20].

We comparatively apply the DFT/RDFT filter bank and the discrete wavelet transform (DWT) to image fusion so as to create new fused images that have more visually satisfactory characteristics. In this section, this is done with image pairs in which each image has defocused subparts. In the next section, we discuss fusion of multispectral and panchromatic remote sensing images.

Because the source images are obtained from a camera which focuses on one of the objects, they have complementary information for those objects. In such applications, image fusion can be performed at three different levels, namely pixel level, feature level, and decision level. In this report, we use pixel level image fusion schemes using max, min, and average value of gray value of pixels from the source images. Figure 10 shows an image fusion scheme based on subband transformation (ST). The inverse subband transformation (IST) recovers the fused image. The subband transformation used is either the DFT/RDFT filter bank or the wavelet transform.

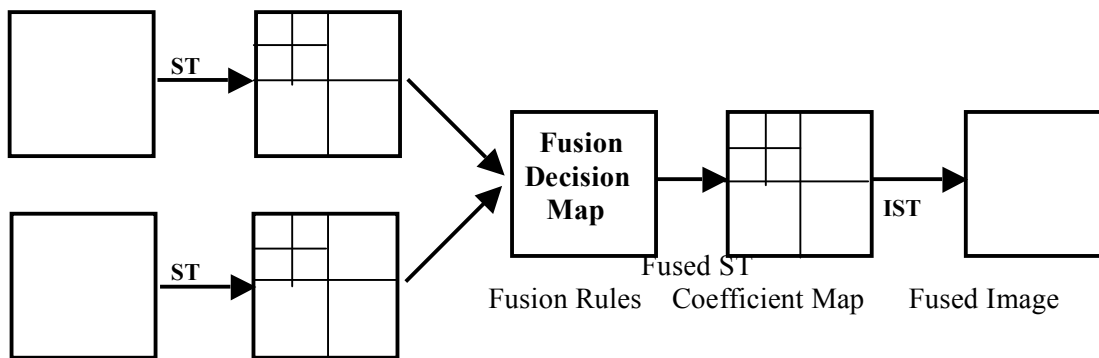


Figure 10. The scheme of image fusion.

6.3.1 Image Set 1

The source images are shown in Figures 11 and 12. Figure 11 shows that the big clock is clearly visible whereas the small clock is blurry. Figure 12 has big blurry clock with small clear clock. The main task of image fusion for these images is how to get an image which is clear for both clocks.



Figure 11. Source image A.



Figure 12. Source image B.

We performed image fusion experiments using pixel level fusion rules by taking maximum, minimum, and average values from source images at decomposition level equal to 3. The experimental results are shown below.

DFT/RDFT Results

Figure 13(a) through Figure 13(d). shows the results. The best result was obtained by averaging the average result with the max result as seen in Figure 13(d).



Figure 13(a). Average result.



Figure 13 (b). Max result.



Figure 13(c). Min result.



Figure 13(d). Max + Average result.

DWT Results

Figure 14(a) through Figure 14(d). shows the results. The best result was obtained by averaging the average result with the max result as seen in Figure 14(d).

Comparing figures 13 and 14, the results with the DFT/RDFT method appear to be visually more satisfactory than the DWT results.



Figure 14(a). Average result.



Figure 14(b). Max result.

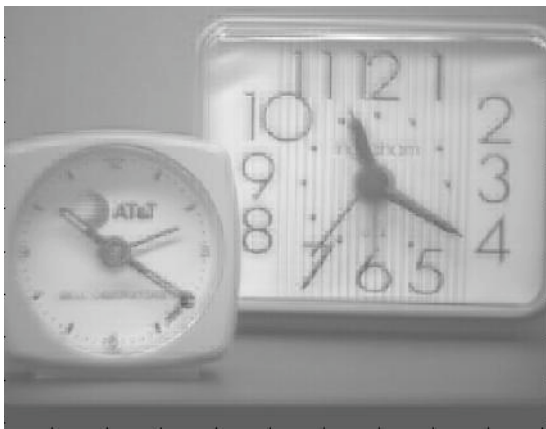


Figure 14(c). Min result.



Figure 14(d). Max + average result.

6.3.2. Image Set 2

The original image used is shown in Figure 15. This is the reference image used when RMSE or PSNR is computed as discussed below. The original image was blurred in the upper and lower portions as seen in Figures 16 and 17 to obtain two partially blurred images.

We again performed image fusion experiments using pixel level fusion rules by taking maximum, minimum, and average values from source images at decomposition level equal to 3. The experimental results are shown below.

DFT/RDFT Results

Figure 18(a) through Figure 18(d). shows the results. The best result was obtained by averaging the average result with the max result as seen in Figure 18(d).

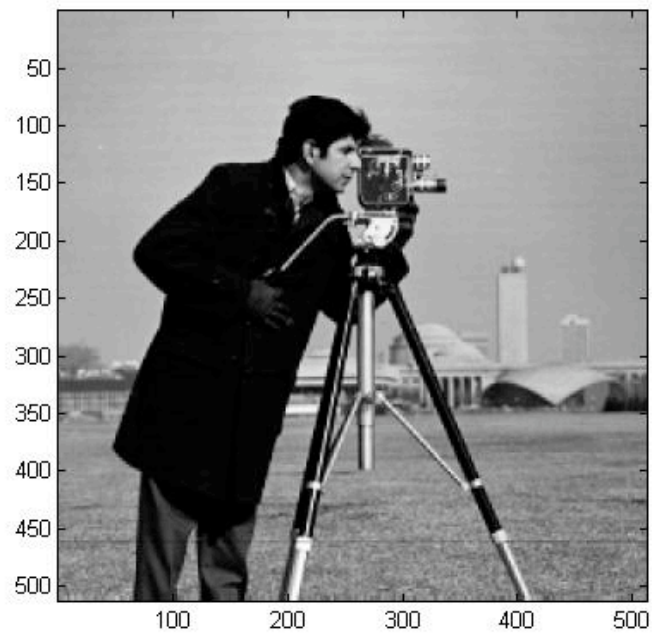


Figure 15. The original cameraman image.

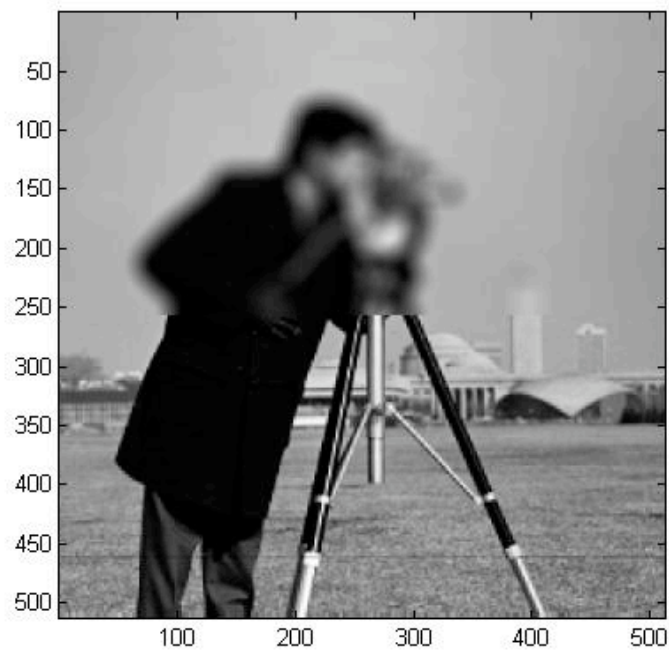


Figure 16. The original cameraman image with the upper portion blurred.

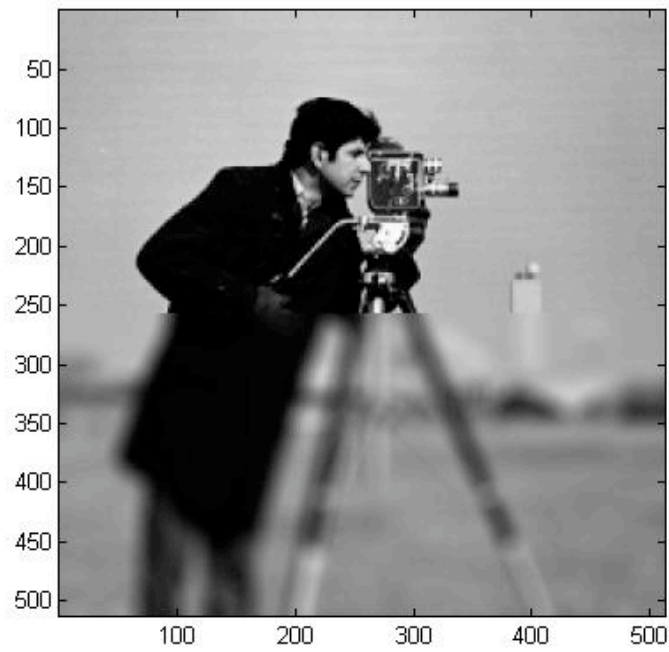


Figure 17. The original cameraman image with the lower portion blurred.

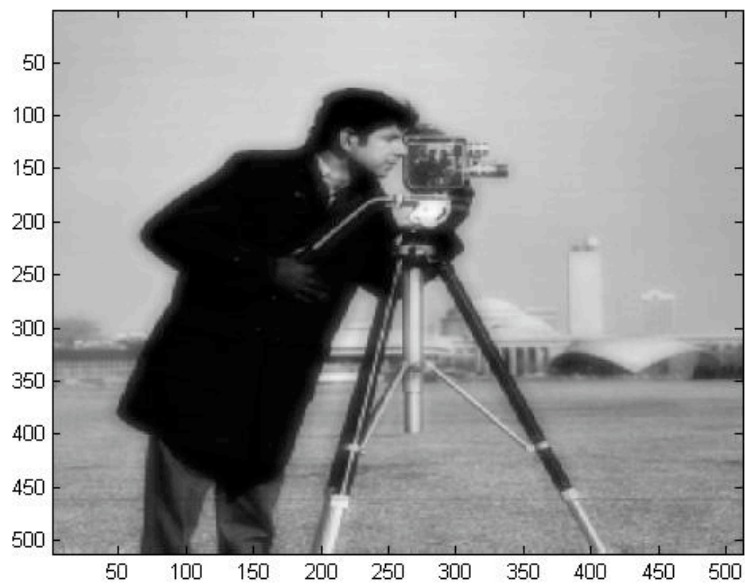


Figure 18(a). Average result.



Figure 18(b). Max result.



Figure 18(c). Min result.



Figure 18(d). Max + average result.

DWT Results

Figure 19(a) through Figure 19(d). shows the results. The best result was obtained by averaging the average result with the max result as seen in Figure 19(d).

Comparing figures 18 and 19, the results with the DFT/RDFT method appear to be visually more satisfactory than the DWT results.

The results with the DFT/RDFT method and the DWT method were also comparatively investigated in terms of root mean square error (RMSE) and peak signal-to-noise ratio (PSNR).

$$\text{RMSE} = \sqrt{\sum_{i=1}^N \sum_{j=1}^N [f(i,j) - F(i,j)]^2} / N \quad (5.1)$$

where $f(i,j)$ is the reference image, and $F(i,j)$ is the fused image, and

$$\text{PSNR} = 20 \log_{10}(255 / \text{RMSE}) \quad (5.2)$$

The corresponding results are shown in Table 1. It is again observed that the DFT/RDFT results are better than the DWT results.



Figure 19(a). Average result.



Figure 19(b). Max result.



Figure 19(c). Min result.



Figure 19(d). Max + average result.

6.4 Fusion of Remote Sensing Images

In remote sensing applications, a panchromatic image which has high spatial resolution may be fused with a lower resolution multispectral image. For example, by merging Landsat thematic mapper TM data which have six reflective 30 meter resolution bands with SPOT panchromatic image which has 10 meter

Table.1 Comparative results of image fusion.

Type	Fusion method	PSNR	RMSE
DFT/RDFT	Max	27.1491	125.3634
	Min	27.0114	129.4007
	Average	27.2690	121.9500
	Max + Average	27.2690	121.9500
DWT	Max	24.4446	233.6786
	Min	24.0804	254.1216
	Average	27.2690	121.9500
	Max + Average	26.4480	147.3268

resolution, one may be able to obtain high spatial resolution multispectral data. Conventional methods for this purpose in remote sensing applications are the intensity-hue-saturation (IHS) transform, the principal component analysis (PCA), and the wavelet transform [17, [18], [19]]. The wavelet transform based methods perform a multiresolution decomposition on each source image, integrate them using a predefined rule, and obtain the reconstructed image by using an inverse multiresolution transform [19]. The discrete wavelet transform (DWT) uses a down-sampling process yielding a multiresolution decomposition which is shift variant. This causes distortion in the final fused images. To prevent this, stationary wavelet transform (SWT) based fusion algorithms have been proposed. The subband decomposition technique described above is used in image fusion in a tree structure consisting of a number of decomposition levels as discussed in Section 5.

In this work, the Landsat TM image and SPOT PAN image of Istanbul shown in Figures 20 and 21 were fused together. First, the Landsat TM image which belongs to Istanbul is geometrically registered onto the SPOT PAN image which belongs to the same area. The Landsat TM image which has 30 meter spatial resolution is super-sampled to 10 meter resolution so that both the Landsat TM and SPOT PAN images occupy the same geographic space and have the same pixel size.

The image fusion algorithm is different from the algorithm used in Section 5.3, and consists of the following steps:

1. Both images are decomposed using subband decomposition. The decomposition level is chosen as 2.

We define the following:

$P_{LL}^j, P_{LH}^j, P_{HL}^j, P_{HH}^j$: j^{th} level LL, LH, HL and HH subbands of the SPOT PAN image, respectively.

TM_{LL}^j , TM_{LH}^j , TM_{HL}^j , TM_{HH}^j : j^{th} level LL, LH, HL and HH subbands of the Landsat TM images, respectively.

2 The approximation subband of the Landsat TM image and the detail subbands of the SPOT PAN image are merged together as

$$F_{LL}^j = TM_{LL}^j$$

$$F_{LH}^j = P_{LH}^j$$

$$F_{HL}^j = P_{HL}^j$$

$$F_{HH}^j = P_{HH}^j$$

where F_{LL}^j , F_{LH}^j , F_{HL}^j , F_{HH}^j correspond to j^{th} level LL, LH, HL and HH subband images of the fused image.

3. Perform the reconstruction to obtain the fused image.

The experiments were carried out with the new method in comparison to the DWT-method in the same tree-structure with two levels of decomposition. The wavelet used was the Daubechies wavelet [8].

The fusion results are shown in Figures 22 and 23, respectively. Figures 24 and 25 are zoomed sections of the corresponding images. It is observed that the RDFT-based image has sharper details and is visually more satisfactory than the DWT-based image.

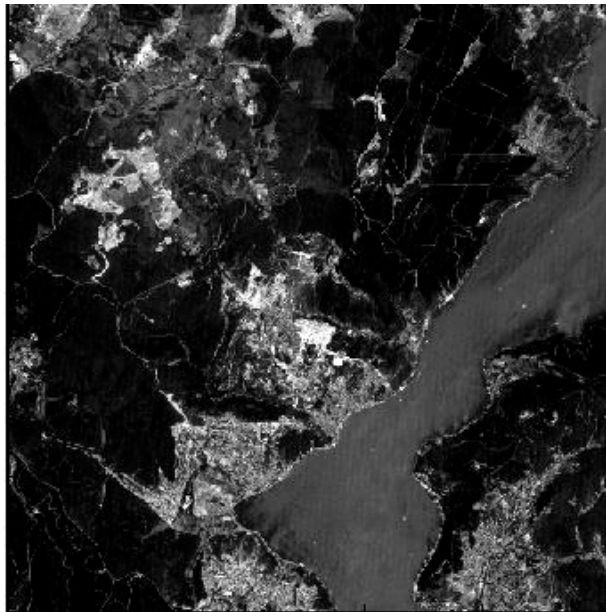


Figure 20. Panchromatic image of Istanbul.



Figure 21. Multispectral image of Istanbul.

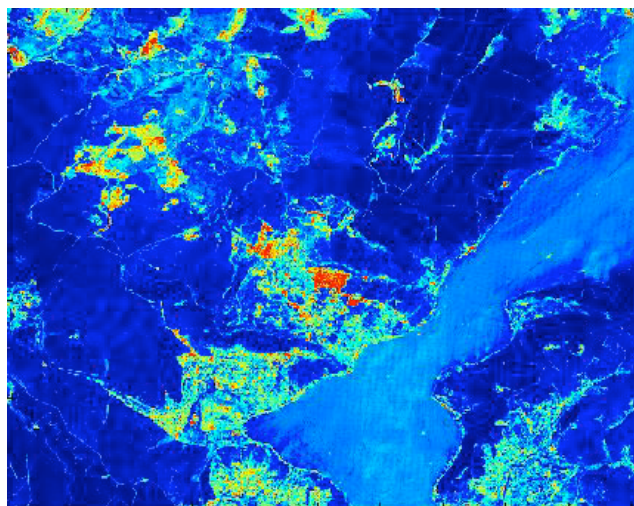


Figure 22. Fused image with the DFT/RDFT method.

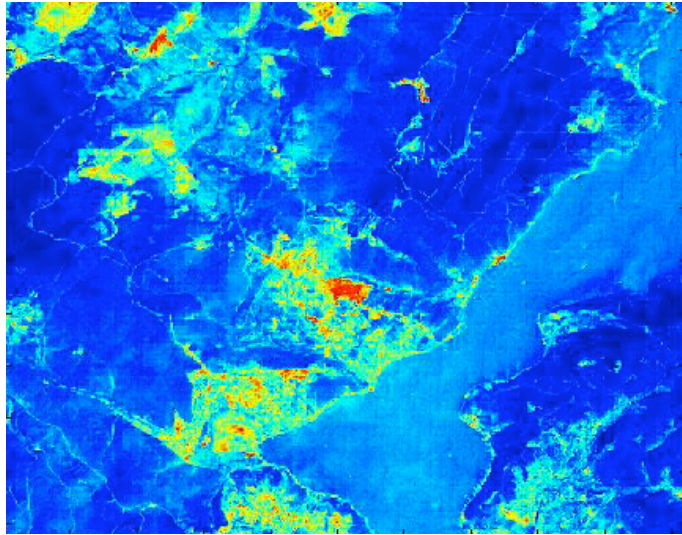


Figure 23. Fused image with the DWT method.

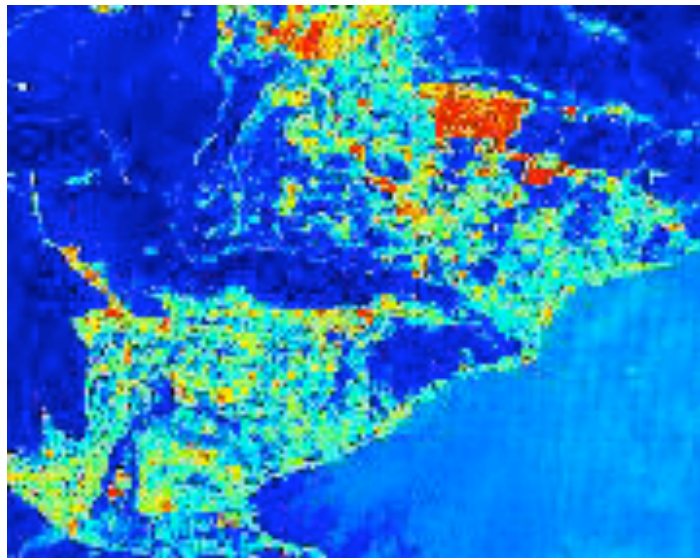


Figure 24. A zoomed section of the fused image with the DFT/RDFT method.

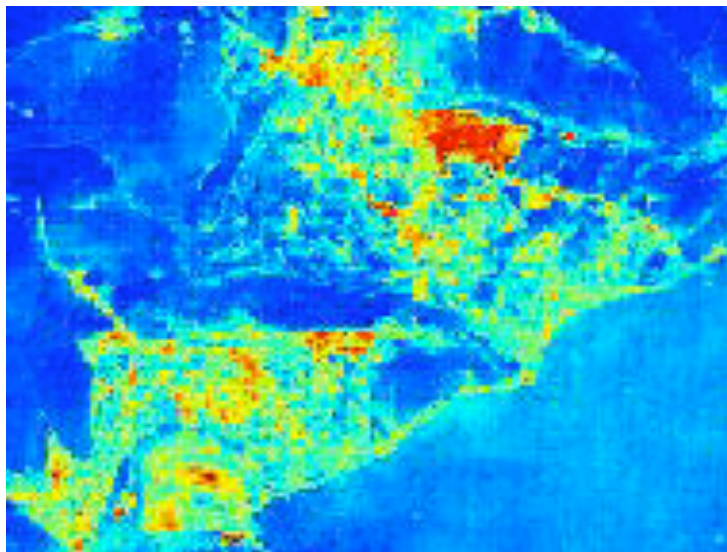


Figure 25. A zoomed section of the fused image with the DWT method.

7. CONCLUSIONS

In this paper, we have developed DFT/RDFT filter banks with non-overlapping symmetric zero-phase analysis/synthesis filters with perfect reconstruction property. The method proposed in the paper was verified with a speech signal and next investigated in image fusion applications, comparatively with the DWT using the Daubechies 1 (Haar) wavelet.

The results obtained with the DFT/RDFT filter bank method were better than the DWT results in all the applications studied. However, the DFT/RDFT method should be compared to other wavelets before more general conclusions can be reached.

In the near future, the targeted research will also involve other types of transforms, and nonstationarity issues.

ACKNOWLEDGEMENT: Jaebang Kim and Murat Sezgin are thanked for their help in parts of this research.

REFERENCES

- [1] R.D. Koilpillai and P.P. Vaidyanathan, "Cosine-modulated FIR filter banks satisfying perfect reconstruction," *IEEE Trans. Signal Processing*, vol. 40, pp.770-783, Apr. 1992.
- [2] R. Gopinath and C. Burrus, "Theory of modulated filter banks modulated wavelet tight frames," in *Proc. IEEE Int. Conf. Acoustics, Speech, and Signal Processing*, Minneapolis, MN, Apr. 1993, pp. 169-172.
- [3] P.P. Vaidyanathan, *Multirate Systems and Filter Banks*. Prentice-Hall, 1993
- [4] T.Q.Nguyen and R.D.Koilpillai, "The theory and design of arbitrary-length cosine-modulated filter banks and wavelets satisfying perfect reconstruction," *IEEE Trans. Signal Processing*, vol. 44, pp.473-483, Mar. 1996.
- [5] N.J.Fliege, "Computational efficiency of modified DFT-polyphase filter banks," in *Proc. 27th Asilomar Conf. Signals, Systems and Computers*, Asilomar, Nov. 1993, pp. 1296-1300.
- [6] Tanja Karp, N.J.Fliege, "Modified DFT filter banks with perfect reconstruction," in *Proc. IEEE Int. Symp. Circuits and Systems*, Seattle, WA, May1995, pp. 744-747.
- [7] Tanja Karp, N.J.Fliege, "Modified DFT filter banks with perfect reconstruction," *IEEE Trans. Circuits and Systems*, Nov. 1999, vol.46, pp. 1404-1414
- [8] M. Vetterli and C.Herley, "Wavelets and filter banks: Theory and design," *IEEE Trans. on Acoustics, Speech, and Signal Proc.*,1992
- [9] Gilbert Strang and Truong Nguyen, *Wavelets and Filter Banks*, Wellesley-Cambridge Press, 1996
- [10] T.G.Marshall, JR, "Zero-phase filter bank and wavelet code r matrices: properties, triangular decompositions, and a fast algorithm," *Multidimensional systems and signal processing*, pp. 71-88, 1997.
- [11] Stephane Mallat, *A Wavelet Tour of Signal Processing*, Academic Press, 1999
- [12] O.Hermann, "On the approximation problem in non-recursive digital filter design," *IEEE Trans. on Circuit Theory*, vol.CT-18, 1971, pp. 411-413.
- [13] J.H. McClellan, T.W. Parks, and L.R. Rabiner, "A computer program for designing optimum FIR linear phase digital filters," *IEEE Transactions on Audio Electroacoustics*, Vol. AU21, pp. 506-526, 1973.
- [14] John G. Proakis and Dimitris G.Manolakis, *Digital Signal Processing: Principles, Algorithms, and Applications*, Prentice-Hall, 1996.
- [15] O. K. Ersoy, "Real discrete Fourier transform," *IEEE Tran. Acoustics, Speech, Signal Proc*, Vol. ASSP-33, No. 4, pp. 880-882, August 1985.
- [16] O. K. Ersoy, "A Comparative review of real and complex Fourier-related transforms," *IEEE Proceedings* , Vol. 82, No. 3, pp. 429-447, March 1994.

- [17] D. L. Hall, J. Lians, “An introduction to multisensor data fusion”, *IEEE Proceedings*, Vol. 85, No. 1, pp. 6-23, 1997.
- [18] C. Pohl, “Multisensor image fusion in remote sensing: concepts, methods and applications”, *International Journal of Remote Sensing*, Vol.19, No. 5, pp. 823-854, 1998.
- [19] W. J. Carper, T. W. Lillesand, R. W. Kieffer, “The use of intensity-hue-saturation transformation for merging SPOT panchromatic and multispectral image data”, *Photogrammetric Engineering and Remote Sensing*, Vol. 56, No. 4), pp. 459-467, 1990.
- [20] G. Pajares, J. M. Dela Cruz, “ A wavelet –based image fusion tutorial”, *Pattern Recognition*, Vol. 37, No. 9, pp. 1855-1872, 2004.